Protein Expression and Purification 174 (2020) 105679

Contents lists available at ScienceDirect

Protein Expression and Purification

journal homepage: www.elsevier.com/locate/yprep

Highly secretory expression of recombinant cowpea chlorotic mottle virus capsid proteins in *Pichia pastoris* and in-vitro encapsulation of ruthenium nanoparticles for catalysis

Jie Zhu[a,*], Kun Yang[a], Aijie Liu[b,1], Xiaoxue Lu[a], Linsong Yang[a], Qinghuan Zhao[a,c,**]

[a] National-Local Joint Engineering Research Center of Biomass Refining and High-Quality Utilization, Changzhou University, Changzhou, 213164, China
[b] Department of Biomolecular Nanotechnology, MESA+ Institute for Nanotechnology, University of Twente, Enschede, 7500 AE, the Netherlands
[c] Suzhou BioTOP Technical Service Co., Ltd., Suzhou Industrial Park, 215123, China

ARTICLE INFO

Keywords:
Pichia pastoris
Cowpea chlorotic mottle virus
Secretion
Virus-like particles
Hybrid nanocatalyst
4-Nitrophenol reduction

ABSTRACT

The applications of viral protein cages have expanded rapidly into the fields of bionanotechnology and materials science. However, the low-cost production of viral capsid proteins (CPs) on a large scale is always a challenge. Herein, we develop a highly efficient expression system by constructing recombinant *Pichia pastoris* cells as a "factory" for the secretion of soluble cowpea chlorotic mottle virus (CCMV) CPs. Under optimal induction conditions (0.9 mg/mL of methanol concentration at 30 °C for 96 h), a high yield of approximately 95 mg/L of CCMV CPs was harvested from the fermentation supernatant with CPs purity > 90%, which has significantly simplified the rest of the purification process. The resultant CPs are employed to encapsulate Ruthenium (Ru) nanoparticles (NPs) via in-vitro self-assembly to prepare hybrid nanocatalyst, i.e. Ru@virus-like particles (VLPs). The catalytic activity over Ru@VLPs was evaluated by reducing 4-nitrophenol (4-NP) to 4-aminophenol (4-AP). The results indicate that, with the protection of protein cages, Ru NPs were highly stabilized during the catalytic reaction. This results in enhanced catalytic activity (reaction rate constant $k = 0.14\ min^{-1}$) in comparison with unsupported citrate-stabilized Ru NPs (Ru-CA) ($k = 0.08\ min^{-1}$). Additionally, comparatively lower activation energy over Ru@VLPs (approximately 32 kJ/mol) than that over Ru-CA (approximately 39 kJ/mol) could be attributed to the synergistic effect between Ru NPs and some functional groups such as amino groups ($–NH_2$) on CPs that weakened the activation barrier of 4-NP reduction. Therefore, enhanced activity and decreased activation energy over Ru@VLPs demonstrated the superiority of Ru@VLPs to unsupported Ru-CA.

1. Introduction

Virus-like particles (VLPs), a class of self-assembled nanocages from viral capsid proteins (CPs), possess several significant characteristics: They are reproducible, robust, and monodisperse hollow scaffolds with highly organized structures. In addition to their use in the development of viral vaccines [1,2], VLPs have garnered considerable attention recently for their application in nanoreactors [3,4], biosensors [5–7], and drug delivery systems [8,9]. In contrast to VLPs that are derived from animal viruses, those derived from plant viruses are safer for us because we cannot be infected by these pathogens. Hence, several plant viruses, such as cowpea chlorotic mottle virus (CCMV), have been increasingly studied. A native CCMV has an icosahedral capsid (triangulation number T = 3) with an outer diameter of 28 nm and an inner diameter of 18 nm. It is formed of 180 copies of a 20-kDa CP subunit that assembles around RNA [3,10]. A unique characteristic of CCMV that has resulted in extensive interest is that changes in pH or ionic strength can alter the morphology of CCMV protein cage, thus exhibiting disassembly–reassembly behavior in-vitro [11,12]. This interesting feature makes CCMV VLPs a versatile platform for the development of functional nanomaterials in a wide range of applications in the fields of materials science and bionanotechnology [13–16].

To date, CCMV CPs have often been produced by replicating viral particles in plant hosts or expressing them in heterologous expression systems including prokaryotic and eukaryotic ones. For the former method, a long replication period and a tedious separation process are

* Corresponding author.
** Corresponding author. National-Local Joint Engineering Research Center of Biomass Refining and High-Quality Utilization, Changzhou University, Changzhou, 213164, China.
E-mail addresses: zhujie@cczu.edu.cn (J. Zhu), zhaoqh@biotop.com.cn (Q. Zhao).
[1] Present address: Department of Chemistry - Ångström Lab., Uppsala University, Box 523, SE 751 20, Sweden.

https://doi.org/10.1016/j.pep.2020.105679
Received 29 March 2020; Received in revised form 20 May 2020; Accepted 20 May 2020
Available online 10 June 2020
1046-5928/ © 2020 Elsevier Inc. All rights reserved.

required to harvest wild-type CPs from plants, often leading to a low output quantity [17,18]. Therefore, several heterologous expression systems have been designed to overcome those disadvantages. Of these, eukaryotic yeast-based systems (e.g., *Pichia pastoris* [*P. pastoris*]) for expressing CCMV CPs have attracted much attention in recent years [18–21]. Yeast cells have advantages similar to those of prokaryotic cells, such as convenient genetic manipulation, low cost, rapid growth rate, and high cell density for protein expression. More importantly, yeast cells have the capability to induce complex post-translational modifications including proteolytic maturation, glycosylation, and disulfide bond formation [22]. They favor the production of properly folded active proteins, thus avoiding the formation of numerous insoluble inclusion bodies, which are often produced in prokaryotic cells [23–25]. Additionally, yeast cells have the capability to secrete heterologous proteins into a fermentation supernatant. Thus, active proteins can be directly collected from the medium without disrupting the cell. Yeast cells significantly facilitate the subsequent purification process and reduce production costs [25–28]. Thus far, CCMV CPs have been successfully expressed on several *P. pastoris* platforms [18,19,29]. However, they primarily have been intracellularly expressed, leading to multiple purification processes.

Herein, we report a *P. pastoris*-based expression system for the secretion of recombinant CCMV CPs. This system gives a high yield of active CPs (95 mg/L) in the supernatant with a high CPs purity (over 90%). Cell disruption was excluded, which simplified the purification process considerably. Secreted CPs were further employed to encapsulate Ruthenium (Ru) nanoparticles via in-vitro self-assembly to prepare a core-shell hybrid nanocatalyst. The reduction of 4-nitrophenol (4-NP) to 4-aminophenol (4-AP) was selected as a model reaction to estimate the catalytic activity of this nanocatalyst. This study provides a simple and environmentally friendly method for the large-scale production of the protein cages of plant viruses in several emerging industries, such as biopharmaceuticals and nanomaterials.

2. Material and methods

2.1. Strain, plasmid, and materials

P. pastoris CN15349 was acquired from BioTOP (Suzhou, China); Plasmid pPIC9K (Invitrogen, USA) was employed for recombinant protein secretion due to its signal peptide-encoding sequence.

Pfu-DNA polymerase; dNTP; T4 ligase; restriction enzymes, including *EcoR* I, *Avr* II, *SnaB* I, *Not* I, *Sac* I, *Sal* I, and *Bgl* II; DNA; and protein markers were purchased from Fermentas, Canada. Phosphatase was purchased from TaKaRa (Dalian, China). PCR product purification and gel recovery kits were purchased from Watson Biotechnologies (Shanghai, China). A TIANamp yeast DNA kit (Tiangen Biotech, Beijing, China) was employed to isolate genomic DNA from yeast cells. Geneticin G418 was purchased from Aladdin (Shanghai, China) for multicopy recombinant screening.

2.2. Culture media

A yeast extract–peptone–dextrose medium (YEPD, 1 L) consisting of 20 g of peptone, 10 g of yeast extract, and 20 g of dextrose (another 15 g of agar for the solid medium) was employed for yeast screening.

A buffered glycerol–complex medium (BMGY, 1 L) consisting of 10 g of yeast extract, 20 g of peptone, 3 g of K_2HPO_4, 11.8 g of KH_2PO_4, 100 mL of 10 × YNB (13.4 g/L), 1 mL of 500 × biotin (4×10^{-4} g/L) and 10 mL of glycerol was employed for cultivating recombinant *P. pastoris* to a high cell density before the expression of target proteins.

A buffered methanol–complex medium (BMMY, 1 L) consisting of 10 g of yeast extract, 20 g of peptone, 3 g of K_2HPO_4, 11.8 g of KH_2PO_4, 100 mL of 10 × YNB (13.4 g/L), 1 mL of 500 × biotin (4×10^{-4} g/L), and 5 mL of methanol was employed for inducing recombinant *P. pastoris* to secrete target proteins.

2.3. Gene construction of CCMV CP

The gene sequence of CCMV CPs was fully synthesized according to the publicly available nucleotide sequence of CCMV (NCBI accession no. AAA46373.1) [30]. A 6 × His tag sequence was also designed on the N-terminus of CPs for facile purification via Ni-NTA affinity chromatography. The designed gene sequence of CCMV CPs is given in Electronic Supplementary Information (ESI). Then, the constructed nucleotide sequence of CCMV CPs was cloned into *EcoR* I and *Not* I restriction sites of pPIC9K plasmid vector for protein expression (shown in ESI). The obtained recombinant vector was named pPIC9K-CP.

2.4. Recombinant strain construction

First, through electroporation, pPIC9K-CP was transformed into chemically competent cells of yeast strain *P. pastoris* CN15349 for protein induction and expression. Multicopy recombinants were then obtained through aminoglycoside antibiotic geneticin G418 concentration gradient screening (1–6 mg/mL) in the YPD medium. Subsequently, PCR amplification was carried out to screen for positive genomic clones. Finally, the selected recombinant was named *P. pastoris* CN15349-CP. It exhibited Mut^+ phenotype due to its rapid growth in methanol medium.

2.5. CCMV CP secretion

Yeast cells were inoculated in 100 mL of liquid BMGY culture medium at 28 °C and agitated at 250 rpm. When the adsorption of the cell suspension reached 2–6 absorbance units at a wavelength of 600 nm (A_{600}), they were removed from the BMGY medium via centrifugation and re-suspended in 100 mL of the liquid BMMY medium. Cells were cultivated at 15°C-35 °C and agitated at 250 rpm for 24–144 h. Methanol was added to the medium at a final concentration of 0%–2.0% every 24 h to induce *P. pastoris* CN15349-CP to secrete CCMV CPs. At the end of the fermentation, yeast cells were discarded by centrifugation, and the supernatant was collected for the further purification of secreted CPs. Four identical tests were carried out for statistical analysis.

2.6. CCMV CP purifications

Two chromatography methods were employed for CP purification: Ni-NTA affinity and anion exchange. In a typical purification process using the former method, the fermentation supernatant was first concentrated via ultrafiltration (10 kD, Amicon® Ultra-15, Millipore, USA) at 4 °C and 5000 × *g* for 30 min. The concentrate was then filtered through a filter with 45-μm membrane and loaded into a Ni-NTA affinity column (Smart Lifesciences Co., China) that was pre-equilibrated with 10 vol of buffer (0.02 M Tris-HCl, 0.5 M NaCl, pH 7.4). Consecutive elutions were obtained using buffers with imidazole at a gradient concentration (0.02 M Tris-HCl, 0.5 M NaCl, 0–0.25 M imidazole, pH 7.4). Eluents with 10 vol of the column was collected in each elution process.

The purification process using anion exchange chromatography was similar to that of Ni-NTA affinity chromatography. First, an anion exchange column (Suzhou Bogen Bioseparation Technology, BG32-3220-02) was equilibrated with 5 vol of buffer (0.02 M Tris-HCl, 0.1 M NaCl, pH 8.9). The supernatant concentrate was loaded and re-equilibrated in the column. The target protein was eluted by elution buffer (0.02 M Tris-HCl, 1 M NaCl, pH 8.9). Next, the eluates containing recombinant CPs were dialyzed using a dialysis membrane of 8 kDa MWCO (Spectrum Labs, CA, USA) for 24 h at 4 °C in 10 vol of disassembly buffer (0.02 M Tris-HCl, 0.9 M NaCl, 0.001 M DTT, pH 7.4) to retain the CPs. Dialysis buffers were renewed every 8 h. Finally, the purified CPs were stored at 4 °C.

2.7. In-vitro assembly of CCMV CPs to VLPs

The CP self-assembly process was carried out via dialysis for 24 h at 4 °C against 10 vol of assembly buffer (0.1 M NaAc, 0.9 M NaCl, 0.01 M $MgCl_2$, pH 4.8) using a dialysis membrane of 8 kDa MWCO (Spectrum Labs, CA, USA). Assembly buffers were renewed every 8 h, and finally, CPs were reassembled to VLPs.

2.8. Characteristics of CCMV CP secretion and assembled VLPs

SDS-PAGE was employed to analyze the molecular weight (Mw) and purity of secreted CCMV CPs. A UV–vis spectrophotometer (756 S, Lengguang Tech. Co. Ltd., Shanghhai, China) was used to measure the adsorption of the supernatant at 280 nm (A_{280}), and the CP concentration was determined using Equation (1):

$$A_{280} = \varepsilon_{CP} \times b \times c \quad (1)$$

where A_{280} is the adsorption of CCMV CPs in the supernatant at a wavelength of 280 nm; ε_{cp} is the extinction coefficient of CCMV CPs (4.33×10^6 M^{-1} cm^{-1}, according to Ref. [3]); and b and c are the optical path length (1 cm, the width of a cuvette) and CP concentration, respectively.

Transmission electron microscopy (TEM) images were acquired by JEOL JEM 2100PLUS to verify the formation of VLPs that were assembled from CCMV CPs. The sizes of the VLPs were analyzed by measuring 20 randomly selected particles.

2.9. Encapsulation of Ru nanoparticles (Ru NPs) into CCMV VLPs

First, citrate (CA)-stabilized Ru NPs (Ru-CA) were prepared via the colloidal method. Specifically, a $RuCl_3$ aqueous solution (6 mM) was mixed in a sodium CA aqueous solution (1.0 wt%) and stirred for 15 min to maintain the 11:1 M ratio of CA to Ru. Next, a $NaBH_4$ solution (0.1 M) was added to reduce Ru^{3+} and stirred for 5 min to maintain the 5:1 M ratio of $NaBH_4$ to Ru. Thus, the Ru colloid solution was prepared. The sizes of the Ru NPs were analyzed by measuring 50 randomly selected particles.

The encapsulation of Ru NPs in CCMV VLPs was conducted as follows: CP dispersion (0.4 mg/mL) was mixed with a Ru-CA solution (6 mM). The solution was well mixed for 30 min and then dialyzed in an assembly buffer at 4 °C overnight. As-prepared CCMV VLPs that had encapsulated Ru NPs were named Ru@VLPs. The sizes of Ru@VLPs were analyzed by measuring 20 randomly selected particles.

2.10. Catalytic performance over Ru@VLPs for the reduction of 4-NP

Catalytic activity over hybrid nanocatalyst Ru@VLPs was estimated according to the reduction of 4-NP to 4-AP, as shown in Scheme 1. The result was compared with that of unsupported Ru colloidal NPs (Ru-CA). The experiments were conducted in a 96-well plate. Specifically, 30 μL of a 4-NP aqueous solution (1 mM) and 20 μL of a Ru@VLP aqueous solution (1.7 μM Ru) were fully mixed in the wells of the plate. The reaction began once 150 μL of the $NaBH_4$ aqueous solution (16 mM) was added to the mixed solution. Real-time data was monitored by a microplate reader (Spark 10 M, Tecan, Switzerland) at a wavelength ranging from 200 to 500 nm. The reactions proceeded for 15 min. Ru-CA was employed as the control. 4-NP, ionized 4-NP, and final-product 4-AP had the maximal adsorptions at wavelengths of 320, 400, and 296 nm, respectively. It is worth noting that 4-NP can be ionized by adding an excess amount of $NaBH_4$, after which its maximal absorption wavelength increases from 320 to 400 nm. Since the extinction coefficient (ε) of 4-NP is much larger than that of 4-AP, the reaction kinetics for evaluating the catalytic activity of as-prepared catalysts was studied by observing the absorption decrease of 4-NP during the reaction at 400 nm. Hence, the conversion of 4-NP (*Con*) in the reaction was employed to evaluate the catalytic activity over as-prepared catalysts and calculated by Equation (2):

$$Con = \frac{A_{NP}^0 - A_{NP}}{A_{NP}^0} \times 100\% \quad (2)$$

where A_{NP}^0 and A_{NP} are the initial adsorption value of ionized 4-NP and the instant adsorption value during the reaction at $\lambda_{400\ nm}$, respectively. Four identical tests were carried out for statistical analysis.

Since 4-NP hydrogenation is generally considered a pseudo first-order reaction [3,31], apparent reaction rate constants (k) for the reduction of 4-NP were calculated based on the total conversion of 4-NP over Ru catalysts using Equation (3):

$$ln\frac{100}{100 - Con} = k \cdot t \quad (3)$$

where *Con* and t represent the total conversion of 4-NP and reaction time, respectively.

Moreover, activation energies for 4-NP hydrogenation over Ru@VLPs and Ru-CA were determined using the Arrhenius equation (Equation [4])

$$lnk = lnA - \frac{Ea}{RT} \quad (4)$$

where Ea is activation energy, T is reaction temperature, A and R are the frequency factor and ideal gas constant (8.314 J $mol^{-1} \cdot K^{-1}$), respectively.

Finally, four runs of Ru@VLP recycling was carried out in a 15-mL autoclave. The total volume of the reaction system was 5 mL. Specifically, 750 μL of the 4-NP aqueous solution (1 mM) and 500 μl of the Ru@VLP aqueous solution (1.7 μM Ru) were fully mixed in the autoclave. The reaction began once 3.5 mL of $NaBH_4$ (16 mM) was added to the mixture. The reaction proceeded at 30 °C for 10 min. At the end of the reaction, the solution was dialyzed for 24 h at 4 °C against 10 vol of assembly buffer to remove reactants and products. After ultrafiltration, the recycled Ru@VLP was employed for the next run.

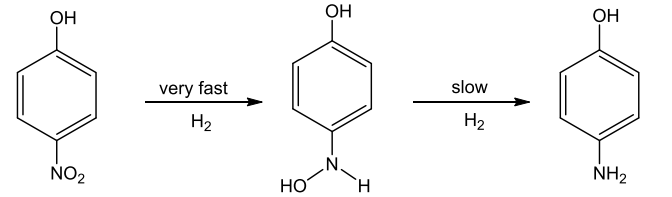

Scheme 1. Reduction of 4-NP to 4-AP.

3. Results and discussion

3.1. Construction of recombinant strain P. pastoris CN15349-CP and secreted CCMV CP expression

Multicopy recombinants containing positive genomic clones were first screened through antibiotic G418 (Figure S1, ESI) and PCR (Figure S2, ESI). The resultant strain *P. pastoris* CN15349-CP was then employed for the secreted expression of recombinant CCMV CPs via two stages: cultivating cells to a high density and secreting CP under methanol induction. At the end of the fermentation, centrifugation was used to discard the yeast cells, and the supernatant was collected for SDS-PAGE analysis. It is obvious that merely two protein bands were discovered in this sample (Lane 1 in Figure S3, ESI). A clear band with a molecular weight of 22 kDa corresponded to the recombinant CCMV CPs, and another light band at 15 kDa likely originated from the culture medium. Results indicate that the purity of secreted CCMV CPs in the fermentation supernatant exceeded 90%. As such, CCMV CPs may

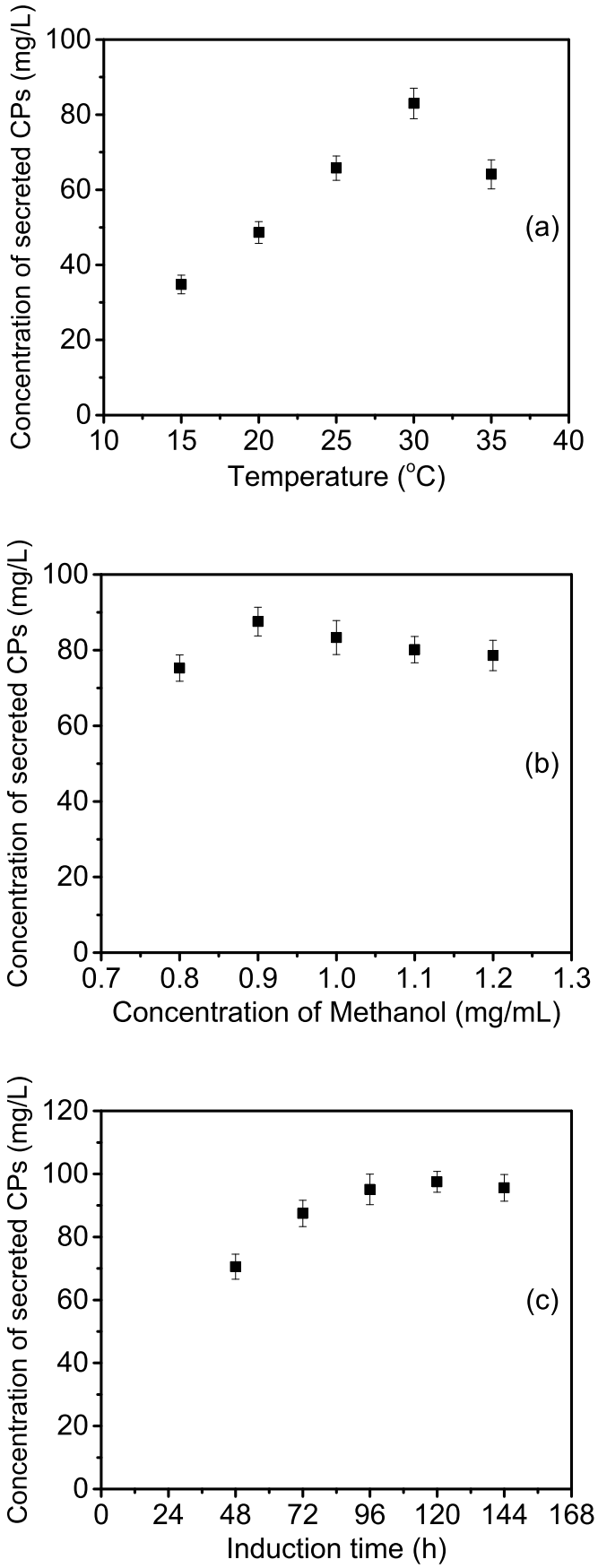

Fig. 1. Concentration of secreted CPs as a function of (a) induction temperature (methanol added to the medium at a final concentration of 1.0% every 24 h; induction time, 72 h), (b) concentration of methanol (induction temperature, 30 °C; induction time, 72 h), and (c) induction time (methanol added to the medium at a final concentration of 0.9% every 24 h; induction temperature, 30 °C). (Mean value: four parallel tests ± standard error).

significantly simplify the downstream purification process.

3.2. Optimization of induction conditions

To improve the yield of secreted CCMV CPs, some induction conditions, including temperature, methanol concentration, and induction time, were optimized. First, various induction temperatures in the range of 15°C-35 °C were used to investigate the effect of temperature on CP secretion. When the temperature was 15°C-30 °C, the amount of secreted CCMV CP clearly increased due to the yeast cells' accelerated metabolism (Fig. 1a). The concentration of secreted CPs in the fermentation supernatant reached a peak (83.0 ± 4.1 mg/L) at 30 °C, similar to the optimal growth temperature for *P. pastoris*. Next, CP expression level decreased dramatically if the induction temperature increased further. Hence, an induction temperature greater than 30 °C inhibited the activity of intracellular alcohol oxidase and the energy levels of cells, improved the cell mortality rate, and increased the negative effects of proteases on protein degradation during the fermentation process. These disadvantages hinder the expression of exogenous proteins [32–35]. Therefore, 30 °C was chosen as the optimal induction temperature for CP secretion.

Next, the methanol concentration was optimized. As shown in Fig. 1b, the concentration of secreted CPs in the fermentation supernatant reached a peak (87.6 ± 3.8 mg/L) at a methanol concentration of 0.9 mg/mL. Methanol, as a bifunctional reagent, is a nutriment that fosters the growth of *P. pastoris* cells and induces the expression of exogenous proteins. When the concentration of methanol is high, the growth of the cells is inhibited due to cytotoxicity, while a low concentration leads to little protein secretion [33,36]. Hence, in this study, the optimal methanol concentration of 0.9 mg/mL can simultaneously meet the requirements of both cell growth and exogenous protein secretion.

In addition, the rate at which cells secreted CPs was positively correlated with induction time. The concentration of secreted CPs reached a high level (95.1 ± 4.8 mg/L) after 96 h (Fig. 1c). However, it only decreased slightly when induction time increased (97.5 ± 3.3 mg/L after 120 h, Fig. 1c). Hence, the capability of cells to secrete proteins continued to decline as nutrients were consumed, products accumulated, and cells aged.

When cost and yield were considered simultaneously, optimal induction conditions were 0.9 mg/mL of methanol concentration at 30 °C for 96 h. Under these conditions, a high yield of approximately 95 mg/L CCMV CPs was harvested from the fermentation supernatant.

Therefore, the secretory expression system we constructed here is simple, efficient, and gives a high yield of active CPs (95 mg/L) in the supernatant with a high CPs purity (over 90%) at a lower cost in comparison with several reported expression systems (summarized in Table 1).

3.3. CCMV CP purification

Anion exchange and Ni-NTA affinity chromatography were used separately to further purify CCMV CPs from the fermentation supernatant. The former process was carried out while considering the different isoelectric points between CCMV CPs (theoretical pI ~9.3 according to ExPASy, Figure S4 in ESI) and other proteins from host cells (pI < 6.0). The results indicate that CCMV CPs can be successfully purified when an elution buffer with a pH of 8.9 is applied. As shown in

Table 1
CCMV CPs expression in several strains.

Expression host (strain, vector)	CPs yield	CPs property	Purification process	Reference
E. coli (BL21, pET23a); E. coli (BL21(DE3), pET28a)	75–100 mg/L	Intracellular expression Inclusions	Cell disruption, denaturation, renaturation, ultracentrifugation	[23,37]
E. coli (Rosetta 2, pET19b)	25.92 mg/L	Intracellular expression Soluble CPs	Cell disruption, affinity chromatography	[25]
Pseudomonas fluorescens (DC487, pDOW3250)	2.6 g/L	Intracellular expression Soluble CPs	Cell disruption, PEG precipitation, sucrose density gradient centrifugation	[24]
Pichia pastoris (pPICZA)	0.05–0.5 mg/g wet cell mass; 4.8 g/L	Intracellular expression Soluble CPs	Cell disruption, PEG precipitation, CsCl gradient centrifugation	[18,19]
Pichia pastoris (pPIC9K)	95 mg/L	Secretion expression Soluble CPs	Anion exchange chromatography	This work

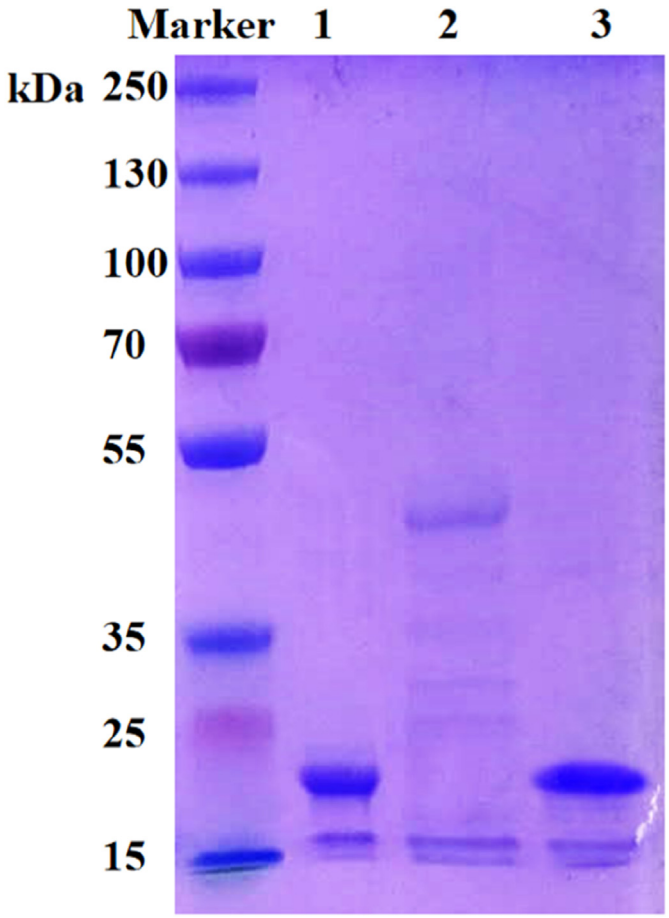

Fig. 2. SDS-PAGE before and after CCMV CP purification by anion exchange chromatography. (Lane 1: fermentation supernatant; Lane 2: effluent after elution using the buffer with 1 M NaCl; Lane 3: effluent during adsorption equilibrium in the column).

Fig. 2, most proteins that originated from host cells were negatively charged at pH 8.9. They primarily adsorbed on anion exchange column (Lane 2). However, CCMV CPs outflowed straightly from the column (Lane 3) due to their electrical neutrality at the same pH.

Additionally, we attempted to use Ni-NTA affinity chromatography for CCMV CP purification due to the design of the N-terminal 6 × His tag in the protein sequence. The eluents were collected and analyzed by SDS-PAGE, as shown in Figure S3 (Lanes 2–8, ESI). Obviously, CCMV CPs were only discovered in the adsorption equilibrium effluent and the elution with 0 mM imidazole (Figure S3, Lanes 2 and 3, ESI). However, no CCMV CPs were found in the effluents that were collected from elution steps, as shown in Figure S3 (Lanes 4–8, ESI), thus indicating that in this study, secreted CPs were difficult to adsorb on the Ni-NTA affinity column. They directly flowed out with effluents. This is possibly related to the structure of CCMV CP. The N-terminal of the CP from wild-type CCMV contains a nine-residue domain that is generally folded toward the interior of the capsid for RNA binding [10]. Therefore, the N-terminal 6 × His tag in recombinant CP might possibly fold the same way, leading to the ineffective purification by Ni-NTA affinity chromatography.

In summary, anion exchange chromatography was an efficient method to purify CCMV CPs, and the purity after said chromatography was performed was > 90%. The purified CPs could be employed for the further encapsulation of Ru NPs.

3.4. In-vitro CCMV CP self-assembly to VLPs and encapsulation of Ru NPs

CCMV CPs were dialyzed in an assembly buffer for 24 h at 4 °C to verify their self-assembly capability to form VLPs in-vitro. The TEM image in Fig. 3a illustrates the successful assembly of CCMV CPs into spherical VLPs with the average size being 27.7 ± 0.6 nm, which corresponds to that of the native CCMV. Assembled VLPs possessed an icosahedral structure, are composed of 180 CP subunits, and have a Caspar–Klug icosahedral triangulation number $T = 3$ [10]. The results prove the strong self-assembly capability of recombinant CCMV CPs.

Fig. 3b illustrates the efficient encapsulation of Ru NPs into CCMV VLPs. The encapsulation rate was approximately 70%, and most VLPs contained several Ru NPs. It is worth noting that the sizes of hybrid Ru@VLPs ranged from 18 to 30 nm with an average size of 22.8 ± 0.6 nm. It can be inferred that the resulting Ru@VLP particles may simultaneously contain assemblies with triangulation numbers $T = 1$, 2, and 3. Specifically, $T = 1$ cages that consist of 60 CP subunits accounted for ~42% of the total (18–22 nm), $T = 2$ cages consisting of 120 CP subunits accounted for ~40% of the total (22–26 nm), and $T = 3$ cages consisting of 180 CP subunits accounted for ~18% of the total (26–30 nm). This relatively large size range may be due to the size variations of encapsulated cargo templates.

The quantity and size ranges of Ru NPs in VLPs were further calculated from the TEM image (Fig. 3b), as shown in Figure S5 (ESI). The results indicate that most Ru@VLPs contained 5–10 Ru NPs. Those containing 6–7 Ru NPs accounted for 50%, the highest proportion of the counted Ru@VLPs (Figure S5a). Ru NPs in VLPs exhibited a narrow size range of 2.5–3.5 nm, with a mean size of 2.72 ± 0.05 nm (Figure S5b). This suggests the protection lent by protein nanocages leads to the high dispersion of Ru NPs.

Therefore, based on above results, the formation path of a Ru@VLP is likely as follows: Upon mixing with CP solution, some Ru NPs partly aggregate due to the increased ionic strength. Aggregates of Ru NPs with different sizes are quickly encapsulated into VLPs via self-assembly due to electrostatic interactions between the two. Thus, Ru NPs are protected by VLPs, hampering any further aggregation. This results in the enhanced stability of Ru NPs. In contrast, unsupported CA-stabilized Ru NPs, i.e., Ru-CA, exist primarily in an aggregated state (Figure S6, ESI). As-prepared hybrid nanocatalysts, i.e., Ru@VLPs, were further

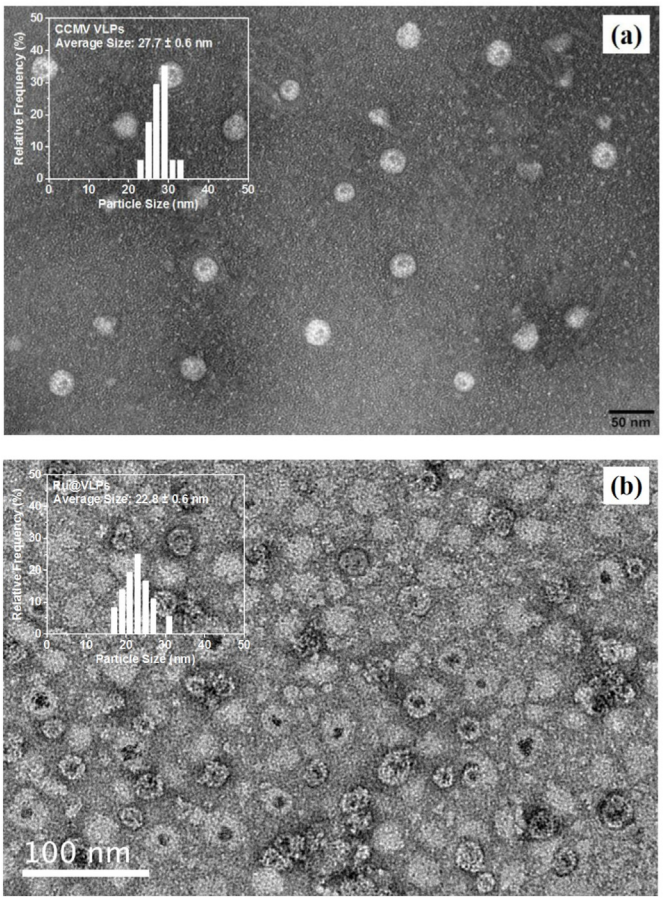

Fig. 3. TEM images of CCMV VLPs (a) and encapsulated Ru NPs (b).

applied in catalysis.

3.5. Catalytic activity of Ru@VLPs on the reduction of 4-NP

The reduction of 4-NP to 4-AP was selected as a model reaction to estimate the catalytic activity of Ru@VLPs (Scheme 1). Since the mechanism of reducing 4-NP is well studied, it is widely applied for investigating the catalytic activity of metallic NPs, hybrid nanostructures, and constituted devices [38–40]. Prior to reaction, the 4-NP solution without $NaBH_4$ has a maximal adsorption at a wavelength of 320 nm. However, by adding an excess amount of $NaBH_4$, 4-NP can be ionized, and its maximal absorption wavelength increases from 320 to 400 nm (Fig. 4a). Simultaneously, 4-NP reduction proceeds, and the resulting final product, 4-AP, reaches a small peak at 296 nm (Fig. 4b). Since the extinction coefficient (ε) of 4-NP is much larger than that of 4-AP, the reaction kinetics for evaluating the catalytic activity of as-prepared catalysts was studied by observing the absorption decrease of 4-NP during the reaction at 400 nm [38].

Fig. 5a indicates the enhanced activity of Ru NPs after their encapsulation into CCMV VLPs. 4-NP conversion over Ru@VLPs, for example, was calculated by Equation (2) to be 93.4% ± 2.7% after 14 min. In contrast, that over Ru-CA was merely 85.8% ± 2.3% after 14 min. The reaction rate constant (k) over Ru@VLPs was further calculated by Equation (3) to be ~0.14 min^{-1} (Figs. 5b), 1.8 times of that over Ru-CA (~0.08 min^{-1}). The improved activity of Ru@VLPs can be reasonably attributed to the enhanced stability of Ru NPs with the protection of CCMV VLPs in comparison with unsupported Ru-CA.

The reaction rate constants over Ru@VLPs and Ru-CA at different temperatures (25°C-40 °C) were further studied, as shown in Figure S7 (ESI). Clearly, as the temperature increased, so did the reaction rates over both catalysts. For example, k over Ru@VLPs increased from 0.14 to 0.30 min^{-1} when the reaction temperature increased from 25 °C to 40 °C. According to the fitting curves in Fig. 6, activation energies (Ea) of 4-NP reduction over Ru@VLPs and Ru-CA were further estimated using Equation (4). The activation energy over Ru@VLPs was calculated to be ~32 kJ/mol, which is lower than that over Ru-CA (~39 kJ/mol). The comparatively lower activation energy over Ru@VLPs can possibly be attributed to the synergistic effect between Ru NPs and some functional groups such as amino groups ($–NH_2$) on CPs that weakened the activation barrier of 4-NP reduction. Therefore, enhanced activity as well as decreased activation energy over Ru@VLPs showed the superiority of Ru@VLPs to Ru-CA.

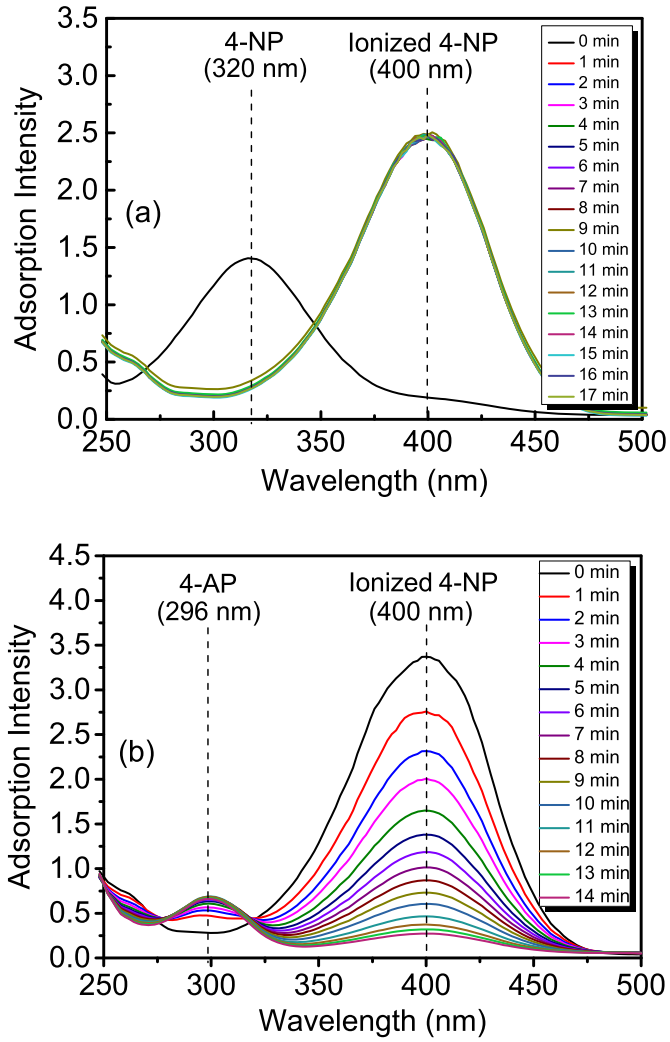

Fig. 4. Real-time data of 4-NP reduction to 4-AP: (a) blank test without any catalysts but with the addition of an excess amount of $NaBH_4$; (b) 4-NP reduction over Ru@VLPs.

3.6. Recycling of Ru@VLPs

Finally, the reusability of Ru@VLPs was examined by recycling them for four runs. The results given in Fig. 7 demonstrate a decline in catalytic activity. For example, 4-NP conversion in the first run was approximately 81.4% ± 3.2% after 10 min. In comparison, it decreased to 68.1% ± 2.7% in the fourth run (less than 4% each run). This occurred primarily due to some mass loss during the recycling process. Hence, as-prepared Ru@VLPs showed good recyclability.

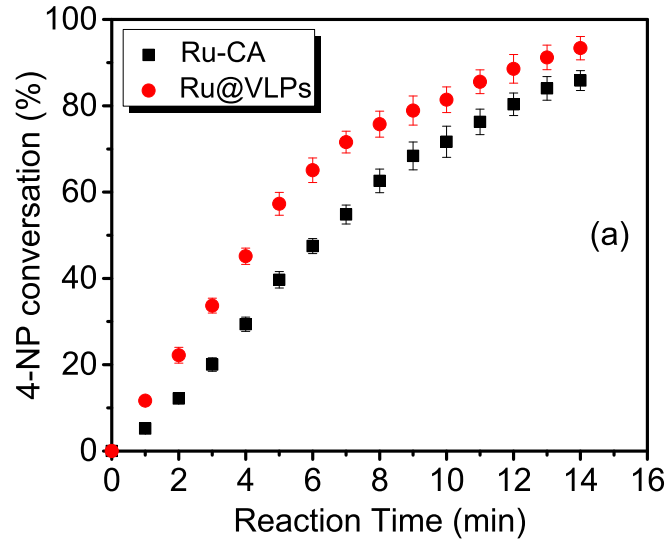

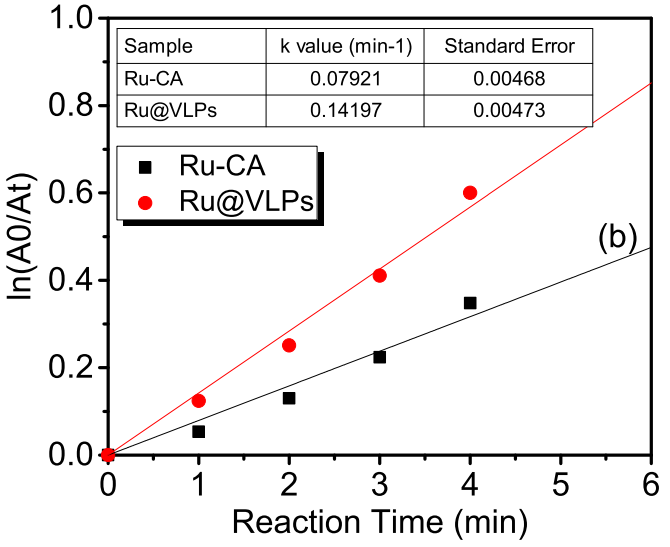

Fig. 5. Catalytic activity of Ru-CA and Ru@VLPs: (a) 4-NP conversion versus reaction time; (b) estimation of reaction rate constants (*k*). (Mean value: four parallel tests ± standard error).

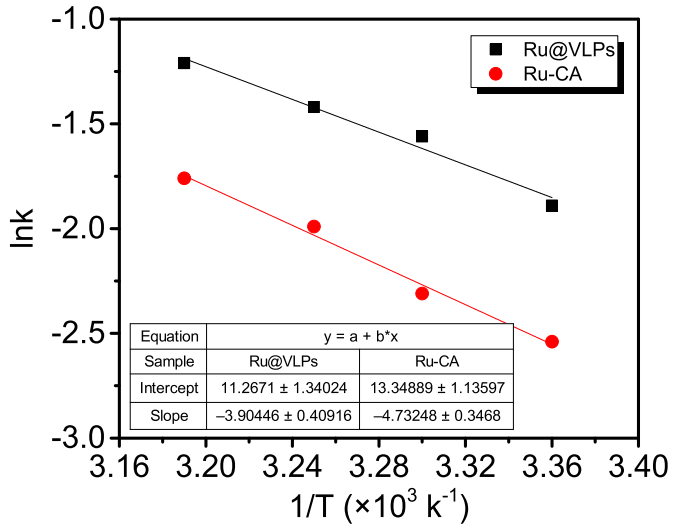

Fig. 6. Estimation of activation energies in 4-NP reduction over Ru@VLPs and Ru-CA.

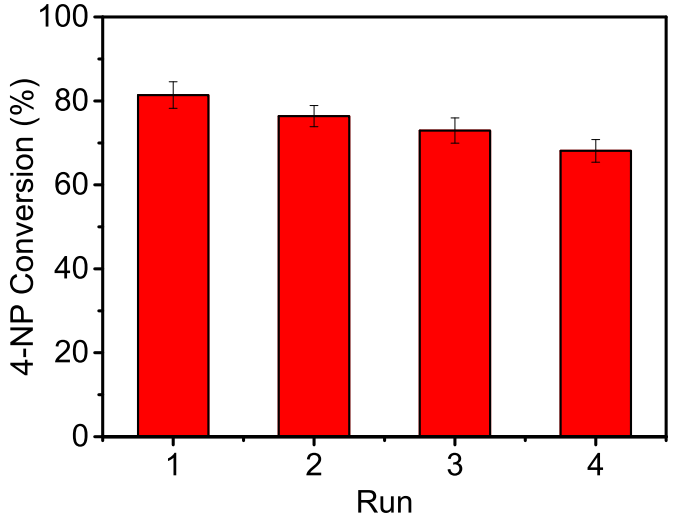

Fig. 7. Recycling of Ru@VLPs for four runs. (Mean value: three parallel tests ± standard error).

4. Conclusion

In summary, we successfully constructed a *P. pastoris*-based expression system for the secretion of recombinant CCMV CPs in a large yield with high purity, thus simplifying the rest of the purification process considerably. The resultant CPs were employed to encapsulate Ru NPs through in-vitro self-assembly to prepare core-shell hybrid nanocatalyst Ru@VLPs. In the reduction of 4-NP to 4-AP, the system exhibited enhanced activity and decreased activation energy in comparison with unsupported Ru-CA, which contributed to the improved stability of Ru NPs with the protection of CCMV VLPs as well as the synergistic effect between the two. In this study, a simple and environmentally friendly method of synthesizing large-scale protein cages of plant viruses was created, which could potentially play a role in emerging industries, such as biopharmaceuticals and nanomaterials.

CRediT authorship contribution statement

Jie Zhu: Supervision, Conceptualization. **Kun Yang:** Investigation. **Aijie Liu:** Writing - original draft. **Xiaoxue Lu:** Investigation. **Linsong Yang:** Validation. **Qinghuan Zhao:** Methodology.

Acknowledgements

This work was supported by the National Natural Science Foundation of China (No. 21676029). The financial support from the Priority Academic Program Development of Jiangsu Higher Education Institutions (PAPD) is also acknowledged.

Appendix A. Supplementary data

Supplementary data related to this article can be found at https://doi.org/10.1016/j.pep.2020.105679.

References

[1] T. Li, H. Lin, Y. Zhang, M. Li, D. Wang, Y. Che, Y. Zhu, S. Li, J. Zhang, S. Ge, Q. Zhao, N. Xia, Improved characteristics and protective efficacy in an animal model of *E. coli*-derived recombinant double-layered rotavirus virus-like particles, Vaccine 32 (2014) 1921–1931, https://doi.org/10.1016/j.vaccine.2014.01.093.
[2] J. Liu, S. Dai, M. Wang, Z. Hu, H. Wang, F. Deng, Virus like particle-based vaccines against emerging infectious disease viruses, Virol. Sin. 21 (2016) 279–287, https://doi.org/10.1007/s12250-016-3756-y.

[3] A. Liu, C.H.H. Traulsen, J.J.L.M. Cornelissen, Nitroarene reduction by a virus protein cage based nanoreactor, ACS Catal. 6 (2016) 3084–3091, https://doi.org/10.1021/acscatal.6b00106.
[4] M. Brasch, R.M. Putri, M.V. de Ruiter, D. Luque, M.S.T. Koay, J.R. Caston, J.J.L.M. Cornelissen, Assembling enzymatic cascade pathways inside virus-based nanocages using dual-tasking nucleic acid tags, J. Am. Chem. Soc. 139 (2017) 1512–1519, https://doi.org/10.1021/jacs.6b10948.
[5] Q. Luo, C. Hou, Y. Bai, R. Wang, J. Liu, Protein assembly: versatile approaches to construct highly ordered nanostructures, Chem. Rev. 116 (2016) 13571–13632, https://doi.org/10.1021/acs.chemrev.6b00228.
[6] L. Yang, A. Liu, S. Cao, R.M. Putri, P. Jonkheijm, J.J.L.M. Cornelissen, Self-assembly of proteins: towards supramolecular materials, Chem. Eur J. 22 (2016) 1–14, https://doi.org/10.1002/chem.201601943.
[7] T. Douglas, M. Young, Viruses: making friends with old foes, Science 312 (2006) 873–875, https://doi.org/10.1126/science.1123223.
[8] Y. Lei, Y. Hamada, J. Li, L. Cong, N. Wang, Y. Li, W. Zheng, X. Jiang, Targeted tumor delivery and controlled release of neuronal drugs with ferritin nanoparticles to regulate pancreatic cancer progression, J. Control. Release 232 (2016) 131–142, https://doi.org/10.1016/j.jconrel.2016.03.023.
[9] M.J. Rohovie, M. Nagasawa, J.R. Swartz, Virus-like particles: next-generation nanoparticles for targeted therapeutic delivery, Bioeng. Transl. Med. 2 (2017) 43–57, https://doi.org/10.1002/btm2.10049.
[10] A. de la Escosura, R.J.M. Nolte, J.J.L.M. Cornelissen, Viruses and protein cages as nanocontainers and nanoreactors, J. Mater. Chem. 19 (2009) 2274–2278, https://doi.org/10.1039/B815274H.
[11] J.A. Speir, S. Munshi, G. Wang, T.S. Baker, J.E. Johnson, Structures of the native and swollen forms of cowpea chlorotic mottle virus determined by X-ray crystallography and cryo-electron microscopy, Structure 3 (1995) 63–78, https://doi.org/10.1016/S0969-2126(01)00135-6.
[12] L. Lavelle, J. Michel, M. Gingery, The disassembly, reassembly and stability of CCMV protein capsids, J. Virol. Methods 146 (2007) 311–316, https://doi.org/10.1016/j.jviromet.2007.07.020.
[13] T. Douglas, M. Young, Host-guest encapsulation of materials by assembled virus protein cages, Nature 393 (1998) 152–155, https://doi.org/10.1038/30211.
[14] Y. Zhang, M.S. Ardejani, B.P. Orner, Design and applications of protein-cage-based nanomaterials, Chem. Asian J. 11 (2016) 2814–2828, https://doi.org/10.1002/asia.201600769.
[15] A. Chaudhary, R.D. Yadav, A review on virus protein self-assembly, J. Nanopart. Res. 21 (2019) 254, https://doi.org/10.1007/s11051-019-4669-0.
[16] S. Bhaskar, S. Lim, Engineering protein nanocages as carriers for biomedical applications, NPG Asia Mater. 9 (2017) e371, https://doi.org/10.1038/am.2016.128.
[17] A. Ali, M.J. Roossinck, Rapid and efficient purification of *Cowpea chlorotic mottle virus* by sucrose cushion ultracentrifugation, J. Virol. Methods 141 (2007) 84–86, https://doi.org/10.1016/j.jviromet.2006.11.038.
[18] Y. Wu, H. Yang, H.-J. Shin, Expression and self assembly of cowpea chlorotic mottle virus capsid proteins in Pichia pastoris and encapsulation of fluorescent myoglobin, Mater. Res. Soc. Symp. Proc. 1317 (2011), https://doi.org/10.1557/opl.2011.138 mrsf10-1317-rr03-05.
[19] S. Brumfield, D. Willits, L. Tang, J.E. Johnson, T. Douglas, M. Young, Heterologous expression of the modified coat protein of Cowpea chlorotic mottle bromovirus results in the assembly of protein cages with altered architectures and function, J. Gen. Virol. 85 (2004) 1049–1053, https://doi.org/10.1099/vir.0.19688-0.
[20] Y.Z. Wu, W. Kim, S.-W. Kim, C.-Y. Eom, H.T. Yang, H.J. Shin, Expression and self-assembly of *Heterocapsa circularisquama* RNA virus-like particles synthesized in Pichia pastoris, Chin. Sci. Bull. 57 (2012) 3288–3293, https://doi.org/10.1007/s11434-012-5125-z.
[21] J. Tomé-Amat, L. Fleischer, S.A. Parker, C. L Bardliving, C.A. Batt, Secreted production of assembled Norovirus virus-like particles from *Pichia pastoris*, Microbial, Cell Factories 13 (2014) 134, https://doi.org/10.1186/s12934-014-0134-z.
[22] L.M. Damasceno, C. Huang, C.A. Batt, Protein secretion in *Pichia pastoris* and advances in protein production, Appl. Microbiol. Biotechnol. 93 (2012) 31–39, https://doi.org/10.1007/s00253-011-3654-z.
[23] A. Hassani-Mehraban, S. Creutzburg, L. van Heereveld, R. Kormelink, Feasibility of cowpea chlorotic mottle virus-like particles as scaffold for epitope presentations, BMC Biotechnol. 15 (2015) 80, https://doi.org/10.1186/s12896-015-0180-6.
[24] J.P. Phelps, P. Dao, H. Jin, L. Rasochova, Expression and self-assembly of cowpea chlorotic mottle virus-like particles in *Pseudomonas fluorescens*, J. Biotechnol. 128 (2007) 290–296, https://doi.org/10.1016/j.jbiotec.2006.10.005.
[25] A. Díaz-Valle, Y.M. García-Salcedo, G. Chávez-Calvillo, L. Silva-Rosales, M. Carrillo-Tripp, Highly efficient strategy for the heterologous expression and purification of soluble *cowpea chlorotic mottle virus* capsid protein and in vitro pH-dependent assembly of virus-like particles, J. Virol. Methods 225 (2015) 23–29, https://doi.org/10.1016/j.jviromet.2015.08.023.
[26] C. Arnett, J. Lange, A. Boyd, M. Page, D. Cropek, Expression and secretion of active Moringa oleifera coagulant protein in *Bacillus subtilis*, Appl. Microbiol. Biotechnol. 103 (2019) 9411–9422, https://doi.org/10.1007/s00253-019-10141-5.
[27] R. Freudl, Signal peptides for recombinant protein secretion in bacterial expression systems, Microb. Cell Factories 17 (2018) 52, https://doi.org/10.1186/s12934-018-0901-3.
[28] L. Shi, D. Wang, W. Chan, L. Cheng, Efficient expression and purification of human interferon alpha2b in the methylotrophic yeast, *Pichia pastoris*, Protein Expr, Purif 54 (2007) 220–226, https://doi.org/10.1016/j.pep.2007.03.005.
[29] Y. Wu, J. Li, H. Yang, J. Seoung, H.-D. Lim, G.-J. Kim, H.-J. Shin, Targeted cowpea chlorotic mottle virus-based nanoparticles with tumor-homing peptide F3 for photothermal therapy, Biotechnol. Bioproc. Eng. 22 (2017) 700–708, https://doi.org/10.1007/s12257-017-0443-2.
[30] R.F. Allison, M. Janda, P. Ahlquist, Sequence of cowpea chlorotic mottle virus RNAs 2 and 3 and evidence of a recombination event during bromovirus evolution, Virology 172 (1989) 321–330, https://doi.org/10.1016/0042-6822(89)90134-7.
[31] N.Y. Baran, T. Baran, M. Nasrollahzadeh, R.S. Varma, Pd nanoparticles stabilized on the Schiff base-modified boehmite: catalytic role in Suzuki coupling reaction and reduction of nitroarenes, J. Organomet. Chem. 900 (2019) 120916–120925, https://doi.org/10.1016/j.jorganchem.2019.120916.
[32] N. Lan, R. Zhang, R. Su, Q. Yang, J. Zhang, Optimization of xylanase expression by recombinant *Komagataella phaffii* without methanol, Food Ferment. Ind. 44 (2018) 8–14, https://doi.org/10.13995/j.cnki.11-1802/ts.015358.
[33] X. Liao, M. Chen, W. Xie, S. Han, Y. Lin, Influence of low inducing temperature on foreign protein production in recombinant *Pichia pastoris*, China Brew. 32 (2013) 9–12, https://doi.org/10.3969/j.issn.0254-5071.2013.02.003.
[34] H.-K. Lim, S.-J. Choi, K.-Y. Kim, K.-H. Jung, Dissolved-oxygen-stat controlling two variables for methanol induction of rGuamerin in *Pichia pastoris* and its application to repeated fed-batch, Appl. Microbiol. Biotechnol. 62 (2003) 342–348, https://doi.org/10.1007/s00253-003-1307-6.
[35] O. Cos, R. Ramón, J.L. Montesinos, F. Valero, Operational strategies, monitoring and control of heterologous protein production in the methylotrophic yeast *Pichia pastoris* under different promoters: a review, Microb. Cell Factories 5 (2006) 17, https://doi.org/10.1186/1475-2859-5-17.
[36] M. Jahic, M. Gustavsson, A.-K. Jansen, M. Martinelle, S.-O. Enfors, Analysis and control of proteolysis of a fusion protein in *Pichia pastoris* fed-batch processes, J. Biotechnol. 102 (2003) 45–53, https://doi.org/10.1016/S0168-1656(03)00003-8.
[37] X. Zhao, J.M. Fox, N.H. Olson, T.S. Baker, M.J. Young, *In vitro* assembly of cowpea chlorotic mottle virus from coat protein expressed in *Escherichia coli* and *in vitro*-transcribed viral cDNA, Virology 207 (1995) 486–494, https://doi.org/10.1006/viro.1995.1108.
[38] X. Kong, H. Zhu, C. Chen, G. Huang, Q. Chen, Insights into the reduction of 4-nitrophenol to 4-aminophenol on catalysts, Chem. Phys. Lett. 684 (2017) 148–152, https://doi.org/10.1016/j.cplett.2017.06.049.
[39] A. Fedorczyk, J. Ratajczak, O. Kuzmych, M. Skompska, Kinetic studies of catalytic reduction of 4-nitrophenol with $NaBH_4$ by means of Au nanoparticles dispersed in a conducting polymer matrix, J. Solid State Electrochem. 19 (2015) 2849–2858, https://doi.org/10.1007/s10008-015-2933-5.
[40] R. Ricciardi, J. Huskens, W. Verboom, Influence of the Au/Ag ratio on the catalytic activity of dendrimer-encapsulated bimetallic nanoparticles in microreactors, J. Flow Chem. 5 (2015) 228–233, https://doi.org/10.1556/1846.2015.00018.